SCIENTIFIC REPORTS
nature research

Check for updates

OPEN

Lead-Halide Scalar Couplings in ^{207}Pb NMR of $APbX_3$ Perovskites (A = Cs, Methylammonium, Formamidinium; X = Cl, Br, I)

Marcel Aebli[1,2], Laura Piveteau[1,2,3], Olga Nazarenko[1,2], Bogdan M. Benin[1,2], Franziska Krieg[1,2], René Verel[1] ✉ & Maksym V. Kovalenko[1,2] ✉

Understanding the structure and dynamics of newcomer optoelectronic materials - lead halide perovskites $APbX_3$ [A = Cs, methylammonium ($CH_3NH_3^+$, MA), formamidinium ($CH(NH_2)_2^+$, FA); X = Cl, Br, I] - has been a major research thrust. In this work, new insights could be gained by using ^{207}Pb solid-state nuclear magnetic resonance (NMR) spectroscopy at variable temperatures between 100 and 300 K. The existence of scalar couplings $^1J_{Pb\text{-}Cl}$ of *ca.* 400 Hz and $^1J_{Pb\text{-}Br}$ of *ca.* 2.3 kHz could be confirmed for $MAPbX_3$ and $CsPbX_3$. Diverse and fast structure dynamics, including rotations of A-cations, harmonic and anharmonic vibrations of the lead-halide framework and ionic mobility, affect the resolution of the coupling pattern. ^{207}Pb NMR can therefore be used to detect the structural disorder and phase transitions. Furthermore, by comparing bulk and nanocrystalline $CsPbBr_3$ a greater structural disorder of the $PbBr_6$-octahedra had been confirmed in a nanoscale counterpart, not readily captured by diffraction-based techniques.

Semiconducting lead halide perovskite materials, foremost of $APbX_3$-type [A = Cs, methylammonium ($CH_3NH_3^+$, MA), formamidinium ($CH(NH_2)_2^+$, FA); X = Cl, Br, I], have raised tremendous interest over the past years due to their outstanding optoelectronic properties, which find application in solar cells[1,2], X-ray[3] and gamma detectors[4–6] and light-emitting devices[7–14]. These semiconductors exhibit unusually high defect-tolerance, which is the nearly intrinsic semiconducting behaviour in spite of the high abundance of structural imperfections. Such defect-tolerance had been attributed to the specifics of the electronic structure, crystal structure and structural dynamics[15–21]. It is therefore fundamental to develop an experimental toolset and a related mind-set for studying the local structure and structural dynamics as well as their relationship to the electronic and physical properties of these semiconductors. Solid-state nuclear magnetic resonance (NMR) is a powerful technique for characterizing solid materials. It is complementary to X-ray diffraction, as it is particularly sensitive to the local environment of nuclei. Chemical composition of $APbX_3$ makes these compounds very well suited for NMR, owing to the range of NMR-active nuclei (^1H[22–25], ^2H[22,23,26–28], ^{13}C[22–25,29], ^{14}N[22–27,29], ^{15}N[25,30], ^{133}Cs[29,31], ^{207}Pb[23–25,27,31–33], ^{35}Cl, ^{37}Cl, ^{79}Br, ^{81}Br, ^{127}I)[34]. In this contribution, we focus on ^{207}Pb NMR spectroscopy of $APbX_3$ compounds and report on the existence of scalar lead-halide J-couplings in some of them. $^1J_{Pb\text{-}Cl}$ of *ca.* 400 Hz and $^1J_{Pb\text{-}Br}$ of *ca.* 2.5 kHz have been measured for $MAPbX_3$ and $CsPbX_3$ compounds. For other compounds within the $APbX_3$ family, scalar couplings are elucidated to be on the order of 2–3 kHz but had not been spectrally resolved. The temperature dependence of the couplings correlates with the known reduction of the structural dynamics and ionic mobility in these perovskites[35].

In $APbX_3$ perovskite compounds, corner-sharing lead-halide octahedra form a 3-dimensional (3D) anionic network, charge-stabilized by A-cations filling large 12-fold-coordinated voids in-between the octahedra. Several 3D-polymorphs of these compounds exist, but they differ in the distortion of the lead-halide octahedral lattice (Fig. 1a; see Table S1 for a detailed overview of known structures at various temperatures). This structural data is correlated in the following discussion with our NMR data. The compounds consist of a dynamic inorganic

[1]Department of Chemistry and Applied Biosciences, ETH Zürich, Vladimir-Prelog-Weg 1-5, CH-8093, Switzerland. [2]Empa-Swiss Federal Laboratories for Materials Science and Technology, Dübendorf, Überlandstrasse 129, CH-8600, Switzerland. [3]Present address: Conditions Extrêmes et Matériaux: Haute Température et Irradiation (CEMHTI), UPR 3079 CNRS, Université d'Orléans, 1D Avenue de la Recherche Scientifique, 45071, Orléans, France. ✉e-mail: verelr@ethz.ch; mvkovalenko@ethz.ch

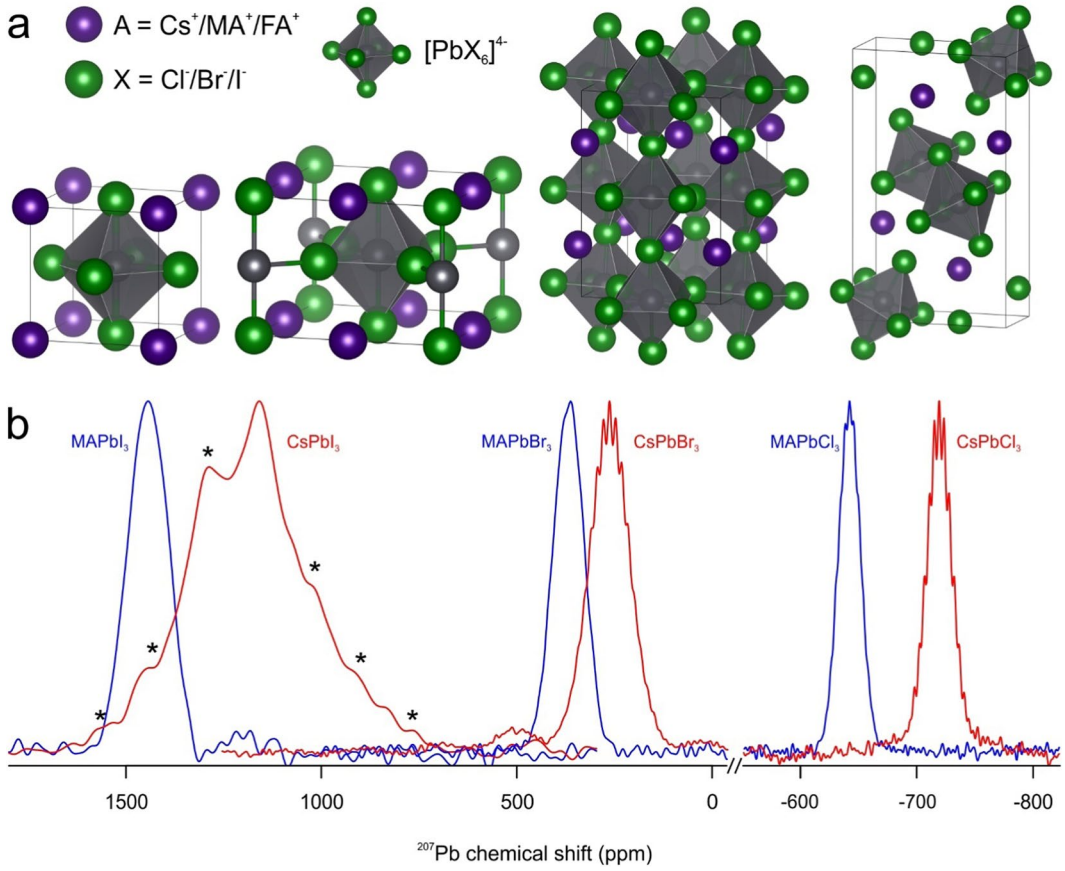

Figure 1. (**a**) Cubic, tetragonal and orthorhombic structures of 3D-perovskites as well as the 1D-structure of orthorhombic $CsPbI_3$. (**b**) ^{207}Pb NMR spectra of $MAPbI_3$, $CsPbI_3$, $MAPbBr_3$, $CsPbBr_3$, $MAPbCl_3$ and $CsPbCl_3$. The spectra of $MAPbI_3$, $CsPbI_3$, $MAPbBr_3$, and $CsPbBr_3$ were acquired at 16.4 T and the spectra of $MAPbCl_3$ and $CsPbCl_3$ were acquired at 11.7 T at room temperature (RT) using powdered materials. Spinning side bands are marked by asterisks.

PbX-framework with a high concentration of point defects (higher than 0.4% in $MAPbI_3$ at room temperature[36]) leading to defect-mediated hopping of the halide anions[37]. These frameworks are coupled through ion-ion interactions and hydrogen bonds to the A-cation. The rotation and displacement of the A-cations lead to distortions and anharmonic vibrations in the whole perovskite structures[38], which has been shown by Whalley *et al.*[39] and Beecher *et al.*[40] for $MAPbI_3$ and by Marronnier *et al.*[41,42] for $CsPbI_3$. All these dynamic processes take place in the picosecond time scale and contribute to the soft structure of the lead halide perovskites. They can be diminished or for some rotations even completely suppressed by reducing the temperature.

NMR studies on lead halide perovskites had already been launched in the 1980s. For $MAPbX_3$, Wasylishen reported in 1985 on the dynamics of the organic cation and phase transitions using ^{2}H and ^{14}N NMR[26]. Most of the subsequent studies concentrated on ^{1}H, ^{2}H, ^{13}C, ^{14}N, ^{15}N nuclei to characterize and understand the dynamics and mobility of the organic cations (MA or FA)[22–27,43–45]. Only a few studies concerned ^{133}Cs NMR[29,31,46–51]. As to the halides, NMR spectroscopy had thus far been hampered by their large quadrupolar constants, leading to massively broadened signals and distorted line shapes[52,53]. For this reason, halides are more commonly assessed with nuclear quadrupole resonance (NQR) spectroscopy[25,44,54–58]. Sharma *et al.*[59] (1987) and the dissertation by Ullmann (1998)[60] are, to our knowledge, the first reports on ^{207}Pb NMR of lead-halide perovskites. Two decades later, ^{207}Pb NMR studies had been resumed by Rosales *et al.*[33], who studied mixed-halide methylammonium perovskites. The last three years have seen the increasing use of ^{207}Pb NMR for the characterization of $APbX_3$ perovskites and novel lead halide compounds[23–25,27,44,45,61–65]. In these studies, $MAPbI_3$ has been the main focus. It was studied at variable temperatures[24,25,27,44], during decomposition[61], with dimethylammonium incorporation[45] and also with bromine substitution[23]. 2D NMR and dynamic nuclear polarization (DNP) NMR was measured for micro- and nanocrystalline $MAPbX_3$ at 100 K, which resulted in an enhancement factor of up to 20 for $MAPbCl_3$[62,65]. $MAPbCl_3$ was additionally measured at various temperatures and its utility as an internal thermometer was shown based on the temperature dependence of its ^{207}Pb NMR chemical shift[63].

Results and Discussion

Of fundamental importance are the first observations of lead-halide J-coupling in $MAPbCl_3$ ($^1J_{Pb\text{-}Cl}$) and in $CsPbBr_3$ as well as Cs_4PbBr_6[27,32]. J-couplings are mediated through bonds by hyperfine interactions between the nuclei and their local electrons. The J-coupling contains information about bond length and angles. It resonates

with the notion that the Pb-halide framework in $APbX_3$ compounds exhibits substantial covalency and directionality in the Pb-X bonding, which is needed for efficient through-bond J-coupling[66]. The existence of these bonds has recently been verified with band structure calculations by Goesten and Hoffmann[67].

Lead-halide J-couplings had already been postulated by Dybowski *et al*. for PbI_2 (built from face-sharing Pb-I octahedra), but could not be resolved[68]. For the ^{207}Pb NMR signal with a full-width at half-maximum (FWHM) of 20 kHz, they calculated a scalar coupling $^1J_{Pb\text{-}I}$ of 4.9 kHz, which is of a similar magnitude as other scalar couplings involving ^{207}Pb[69].

The observation of J-coupling depends on several factors such as nuclear spin and quadrupolar moment of the halide as well as any dynamic changes in the structure or structural defects. The nuclear spin of the halide determines the number of lines present within the coupling pattern, while the large quadrupolar constant of the halides generally broadens the signal and therefore masks the J-coupling[70]. The next factor that affects the observation of J-coupling is a combined effect of structural inhomogeneities that are primarily due to structural dynamics but also to static structural defects. A distribution of chemical sites, which can be caused, for instance, by vacancies or doping, leads to (inhomogeneous) broadening of the lines. Structure dynamics of the lead halide sublattice falls in the picosecond range[35,71], which is too fast for the NMR time scale (µs-to-seconds) and will be averaged out and seen as a quasi-static impact on the observed NMR spectrum. The major type of Pb-halide atomic motion is the tilting of the lead-halide octahedra with respect to each other[72,73]. This constantly changes the Pb-X-Pb bond angle and therefore affects the orbital overlap thus obscuring the J-coupling. We therefore expect that the J-coupling is a sensitive probe for the structural dynamics or disorder. This disorder was also related to the phonon anharmonicity observed in hybrid perovskites[39]. It is also important to note that the dynamic disorder of the A-site cation is correlated to that of the Pb-halide framework[38]. Differences in the Pb-X bond length will result in slightly unequal coupling strengths to the individual halides in the lattice[74]. A perfect PbX_6-octahedron should therefore yield narrower lines compared to a distorted one. This has been shown on ^{207}Pb-^{19}F couplings in amorphous $Pb_5Ga_3F_{19}$[75]. J-couplings to quadrupolar nuclei are known to be self-decoupled, due to their fast relaxation induced by the quadrupole. The fact that in these perovskite materials the couplings are clearly visible, indicates a relatively slow quadrupolar relaxation of the halides[76]. Once observed, the J-coupling could be, in principle, correlated to the atomic structure. While calculations of J-couplings are sufficiently accurate for light elements (^1H, ^{13}C *etc*.) and are generally possible for solid-state inorganic materials[77,78], there is no such theoretical work yet for lead-halide perovskites. At present, a broader experimental survey over diverse lead halide structure is needed to start drawing correlations with the structural motives (bond length/angles, corner/edge/face-sharing connectivity, octahedral or other lead halide building blocks *etc*.).

All studied $APbX_3$ compounds were synthesized using solution-phase methods, as reported earlier (see Supporting Information for synthesis details)[64,79,80]. We note that the as-synthesized 3D-polymorph of $FAPbI_3$ (α-phase) rapidly converts into a face-sharing 1D-polymorph (δ-phase) under magic angle spinning (MAS) NMR and therefore we could acquire the spectrum only under static conditions (Fig. S1)[64]. For $CsPbI_3$, only the 1D-phase (δ-phase) with edge-sharing octahedra is stable at RT[81,82]. $CsPbBr_3$ NCs were synthesized using colloidal methods with long-chain zwitterionic surfactants as surface capping ligands[83]. The NCs were precipitated using antisolvents and properly purified before being isolated by centrifugation, dried under vacuum, and measured as a pure solid.

RT MAS solid-state ^{207}Pb NMR spectra of powdered Cs and MA compounds are displayed in Fig. 1b. In agreement with the earlier reports, no scalar couplings were found neither for $MAPbI_3$ (blue left, Fig. 1b) nor for $MAPbBr_3$ (blue middle, Fig. 1b)[23,24,33,44,59,61,62]. δ-$CsPbI_3$ showed no scalar coupling either (red left, Fig. 1b). However, chloride compounds exhibit pronounced J-couplings of $^1J_{Pb\text{-}Cl} = 400$ Hz in $CsPbCl_3$ (red right, Fig. 1b) and $^1J_{Pb\text{-}Cl} = 390$ Hz in $MAPbCl_3$ (blue right, Fig. 1b). The latter is similar to that reported by Bernard *et al*. earlier[27]. A particularly strong scalar coupling was observed for $CsPbBr_3$; $^1J_{Pb\text{-}Br} = 2.3$ kHz (red middle, Fig. 1b). This shows that Pb-Br scalar couplings are possible and that the ^{207}Pb NMR spectra of $CsPbBr_3$ and Cs_4PbBr_6 acquired and presented in the dissertation of Ullmann appear to exhibit coupling patterns as well although not named and rationalized as such by the author[60]. The coupling patterns observed for $CsPbBr_3$ as well as for $CsPbCl_3$ and $MAPbCl_3$ (Fig. S2) can be safely attributed to scalar coupling since the splitting between the lines stays unchanged at different magnetic fields but changes with temperature (Fig. 2).

The coupling patterns match expectations for lead coordinated to six equivalent halides in an octahedron. Under 1st order conditions, the signal of a nucleus coupled with n magnetically equivalent nuclei of spin I is a multiplet with $2nI + 1$ lines[84]. Accordingly, for six equivalent halides ($n = 6$) with spin $I = {}^3/_2$ (^{35}Cl, ^{37}Cl, ^{79}Br, ^{81}Br) a multiplet with 19 lines is anticipated. The intensity of the individual lines is obtained by constructing a coupling tree for a spin $I = {}^3/_2$, related to Pascal's triangle. The coupling pattern of $CsPbBr_3$ and $MAPbBr_3$ at 100 K were simulated by using the experimental scalar couplings of 2.5 and 2.35 kHz, the theoretical intensities from the coupling tree to six equivalent spins $I = {}^3/_2$ and a Lorentzian line shape with a FWHM of 2.1 and 2.35 kHz. Experimental data and simulations are in excellent agreement (Fig. 2).

Based on the observation that $CsPbBr_3$ and $MAPbBr_3$ possess similar total linewidth in their ^{207}Pb NMR spectra at RT, the hypothesis that an underlying scalar coupling is responsible for the observed overall spectral width is plausible. The absence of visible lines in the multiplet in $MAPbBr_3$ can be explained by the greater broadening of the individual lines. Potential interactions causing such line-broadening in NMR are the dipolar coupling, the chemical shift anisotropy (CSA), site disorder, structural dynamics, and fast relaxation[84]. Since the sample is spun at the magic angle at 10 kHz or faster, dipolar couplings (80–280 Hz for Pb-X, and 25 Hz for Pb-Cs and Pb-Pb) and CSAs are averaged out[85]. In a reference experiment, under static conditions, these two interactions also broaden the lines in the ^{207}Pb NMR spectrum of $CsPbBr_3$ to such an extent that they cannot be resolved anymore (Fig. S3). Hence, we conclude that the site-disorder, dynamics or fast relaxation are greater contributors to the line-broadening in $MAPbBr_3$ and $MAPbI_3$ than they are in $CsPbBr_3$, this way obscuring the J-coupling.

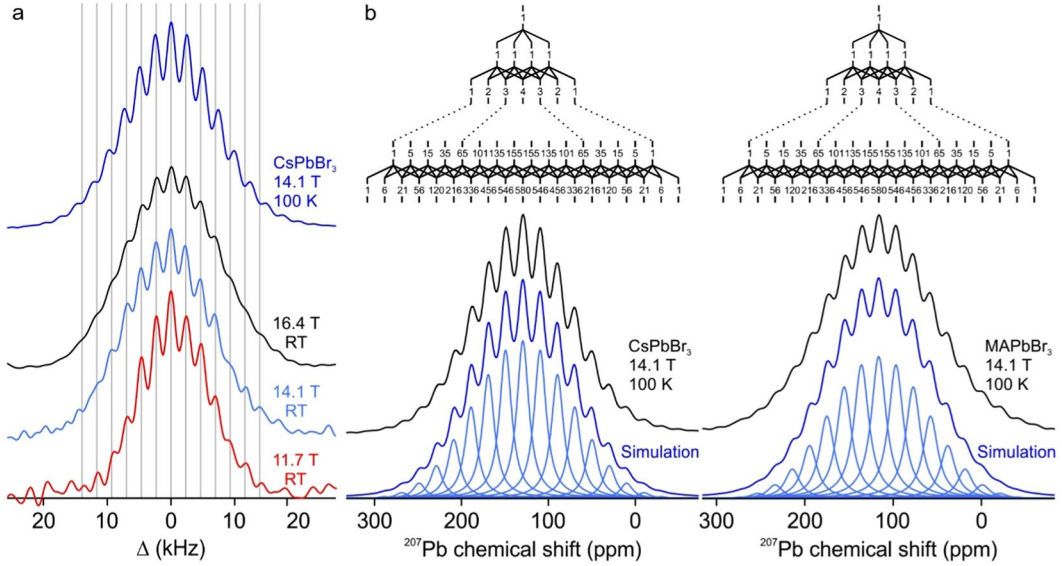

Figure 2. (**a**) ^{207}Pb NMR spectra of $CsPbBr_3$ acquired at 14.1 T at 100 K (dark blue), 16.4 T at RT (black), 14.1 T at RT (light blue) at 11.7 T and RT (red). The grey lines serve as a guide to the eye by marking the lines of the coupling pattern. The spectra are displayed against a frequency axis centered around 0 Hz. This illustrates most clearly the constant splitting distance (in Hz) between lines, due to a scalar coupling of $^1J_{Pb\text{-}Br} = 2.3$ kHz at RT. (**b**) Coupling trees for six equivalent spins $I = {}^3/_2$ (top) and the ^{207}Pb NMR spectra of $CsPbBr_3$ (left) and $MAPbBr_3$ (right) acquired at 100 K on a 14.1 T instrument. The acquired spectra are shown in black. The simulated individual lines with intensities obtained from the coupling trees and scalar couplings of 2.5 and 2.4 kHz for $CsPbBr_3$ and $MAPbBr_3$ respectively are displayed in light blue. The sum of the lines is shown in dark blue and is matching the experimental data.

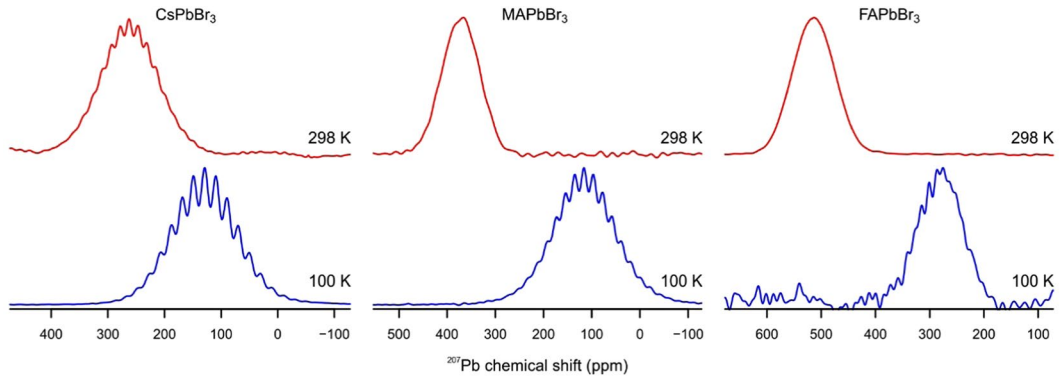

Figure 3. ^{207}Pb NMR spectra of $CsPbBr_3$ (left), $MAPbBr_3$ (middle) and $FAPbBr_3$ (right). The spectra acquired at RT are shown in red (top) and the ones at 100 K in blue (bottom). The isotropic chemical shifts and the coupling constants are listed in Table 1. A possible coupling in $FAPbBr_3$ is difficult to observe due to the low signal-to-noise ratio.

Structural disorder, especially of a dynamic nature, is strongly dependent on temperature in the mobile lead halide lattices as is evidenced by the NMR experiments at low temperatures (Figs. 2 and 3). The low-temperature measurements in this study were carried out at 100 K, since at this temperature all lead halide perovskites are reported to be in their lowest-temperature polymorph. No further phase-transitions were reported to occur below 100 K.

The isotropic chemical shift of all compounds substantially changes towards higher frequencies upon cooling, which is typical for the ^{207}Pb NMR signal. For $CsPbBr_3$, one can clearly observe an improved resolution of the coupling pattern at 100 K (Fig. 3). The FWHM of the individual lines narrows from 2.7 to 2.1 kHz while the coupling strength increases from 2.3 to 2.5 kHz. The stronger coupling can be explained by the contraction of the unit cell that occurs upon cooling leading to a shortening of the Pb-Br bonds[86–88]. A more prominent improvement of the coupling resolution can be observed for $MAPbBr_3$. After the phase transition to the orthorhombic phase below 150 K the coupling pattern appears (Figs. 3 and S4). In this phase, the motion of the MA-cation is limited to rotation around its C-N axis. This has been shown by Wasylishen *et al.*[26] with ^{2}H and ^{14}N NMR, by Zhu *et al.*[35] where the time-resolved

Compound	Temperature	δ_{iso} (ppm)	$^1J_{Pb\text{-}X}$ (Hz)	FWHM lines (Hz)	FWHM total (kHz)
$CsPbCl_3$	RT[a)]	−714	400	600	2.4
$CsPbBr_3$	RT[a)]	262	2300	2400	13.8
	100 K[b)]	130	2500	2100	16.9
$CsPbBr_3$ NCs	RT[a)]	252	—	—	17.6
$CsPbI_3$	RT[a)]	1160	—	—	20.0
	100 K[b)]	990	—	—	25.0
$MAPbCl_3$	RT[a)]	−630	390	600	2.3
$MAPbBr_3$	RT[a)]	365	—	—	13.6
	100 K[b)]	125	2350	2350	16.6
$MAPbI_3$	RT[a)]	1445	—	—	17.6
	100 K[b)]	1030	—	—	20.0
$FAPbBr_3$	RT[a)]	515	—	—	13.1
	100 K[b)]	280	—	—	13.4
$FAPbI_3$	RT[a)]	1515	—	—	22.2

Table 1. ^{207}Pb NMR data of $APbX_3$ perovskites. Acquired under MAS at a) 20 kHz, b) 10 kHz. Spinning at faster MAS increases the temperature of the sample and therefor changes the chemical shift (Fig. S3).

optical Kerr effect at various temperatures was measured and calculated with molecular dynamics simulations by Even *et al.*[89]. In its high-temperature phases, the MA cations can be described as an anisotropic molecular liquid while at 77 K it was found to be frozen. The dynamics of the A-cation and the halides are coupled by hydrogen bonds[37]. A mobile cation with rotational freedom will, therefore, lead to a higher distortion of the PbX_6-octahedra. These distortions are so far only visible in synchrotron methods like total scattering or pair distribution function analysis[90]. In NMR these deformations of the octahedra will result in a smeared out coupling pattern. ^{207}Pb NMR is, therefore, a useful tool to indirectly detect A-cation dynamics and its induced distortion of the inorganic lattice.

For $FAPbBr_3$, no coupling was observed despite cooling, and the total FWHM does not change significantly. This indicates a still highly mobile and disordered surrounding for the ^{207}Pb nuclei. Indeed, it has been shown by single-crystal XRD that the bromides have large displacement factors orthogonal to the Pb-Br bonds even at 100 K[91]. Additionally, by synchrotron XRD, four distinct positions for Br where detected[92]. This displacement, therefore, leads to inhomogeneously broadened lines and obscures the coupling pattern. A fast deformation dynamics in hybrid organic inorganic perovskites was also observed by measuring the hot fluorescence emission[35]. This deformation was attributed to the coupling of the liquid-like motion of the organic cations with the inorganic framework. With ^{207}Pb NMR we could also detect these distortions, present even at 100 K (Fig. 3), making it a powerful method to probe for lattice dynamics at various temperatures. The signal to noise ratio for the low temperature measurement is lower compared to $CsPbBr_3$ and $MAPbBr_3$ measurements, due to the lower number of scans.

The lines of $APbBr_3$ are several times broader than their chlorine analogs (2500 Hz vs. 600 Hz). Both bromine and chlorine possess two isotopes with high natural abundance% ^{35}Cl (76%) and ^{37}Cl (24%) as well as ^{79}Br (51%) and ^{81}Br (49%). The J-couplings between ^{207}Pb and the different isotopes further contribute to the broadening of the individual lines in the coupling pattern, which cannot be quantified at this stage. Another possible contribution to the line broadening could be faster relaxation due to the close vicinity of ^{207}Pb to quadrupoles (halides). All isotopes of chlorine and bromine have a spin of $I = {}^3/_2$, but the quadrupole moments of the bromine isotopes are four times larger than the ones of the chlorine. This effect should be even more severe for iodine in $APbI_3$ perovskites, with a spin of $I = {}^5/_2$ and a quadrupole moment more than twice as large as the bromine. Possible Pb-I couplings were calculated by Dybowski *et al.* in PbI_2 to be around 4.9 kHz and by Bernard *et al.* in $MAPbI_3$ to be between 2 and 3 kHz. So far, none of these couplings could be experimentally resolved.

For $MAPbI_3$, low activation energy for migration of iodine and MA was calculated by Eames *et al.*[36], and confirmed by experimental studies[24,93]. This ion migration will additionally disturb the PbI_6-octahedra. Low-temperature measurements will, therefore, be indispensable for the resolution of Pb-I scalar couplings. At 100 K, a broad tensor was observed for $APbI_3$ (Fig. S5). The isotropic chemical shifts are 990 ppm for $CsPbI_3$ and 1030 ppm for $MAPbI_3$ with FWHM values of around 25 and 20 kHz, respectively. The presence of spinning side bands is an indicator for high anisotropy around the lead nuclei. The spinning side bands overlap complicating the identification of an eventual coupling pattern. Higher spinning speeds would be required to prevent an overlap of the spinning side bands and help resolve the coupling pattern.

Since lead halide couplings were observed for several 3D-perovskite bromides and chlorides, we have looked for the occurrence of $^1J_{Pb\text{-}X}$ couplings in other octahedrally coordinated lead halides, such as the 0D Cs_4PbBr_6. Here too, we could observe a well-resolved coupling of 2.0 kHz was detected even at RT (Fig. 4). The FWHM is 1.5 kHz, which is significantly narrower than that of $CsPbBr_3$ at 2.4 kHz. All Pb-Br bonds are identical in Cs_4PbBr_6 unlike in $CsPbBr_3$, and this leads to a smaller coupling constant distribution that narrows the linewidth[94]. This clearly shows the effect of lattice distortions on the coupling. For a better insight into this effect, the comparison with 0D hybrid materials with MA and FA would be indispensable. Unfortunately, these materials are so far not known.

We have then also probed the effect of dimensionality by comparing bulk material and colloidal nanocrystals (NCs) of $CsPbBr_3$ (Fig. 4). These NCs have recently become an object of intense research due to their outstanding luminescent properties – narrow-band emission with high absolute quantum yields, highly suited for applications

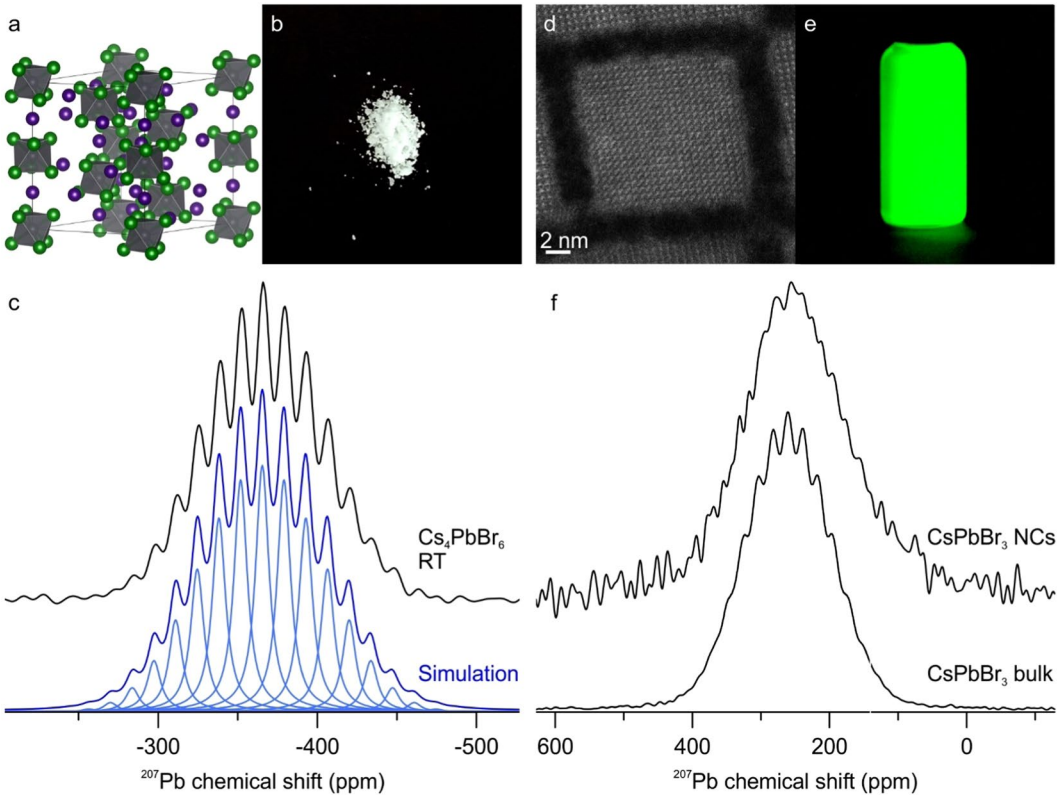

Figure 4. (**a**) Crystal structure of 0D Cs_4PbBr_6 with isolated $PbBr_6$-octahedra. (**b**) Picture of Cs_4PbBr_6 powder. (**c**) ^{207}Pb NMR spectrum of Cs_4PbBr_6 (black) at RT acquired on a 16.4 T spectrometer. The simulated individual lines with intensities obtained from the coupling tree, a FWHM of 1.5 kHz and a scalar coupling of 2.0 kHz are displayed in light blue. The sum of the lines is shown in dark blue and is matching the experimental data. (**d**) High-Angle Annular Dark-Field Scanning Transmission Electron Microscopy (HAADF-STEM) image of a single $CsPbBr_3$ NC. (**e**) Colloidal solution of $CsPbBr_3$ NCs under UV excitation. (**f**) ^{207}Pb NMR spectra of $CsPbBr_3$ bulk (bottom) and NCs (top) acquired at RT on a 11.7 T instrument with identical measurement and processing parameters. The coupling pattern cannot be resolved for the NCs and the total line width increases to 17.6 kHz. This was attributed to higher $PbBr_6$-octahedral disorders over the whole nanocrystal compared to the bulk material.

in television displays[8,21,83]. The coupling cannot be resolved at RT, and the total linewidth increases to 17.6 kHz. This is attributed to higher disorder and higher ion-mobility in NCs. In fact, this result correlates well with the model proposing coherent twins and dynamic disorder in these nanocrystals from the analysis of X-ray total scattering techniques and the Debye scattering equation[95].

Conclusions

In summary, scalar couplings between ^{207}Pb and halide nuclei (^{35}Cl, ^{35}Cl,^{79}Br, ^{81}Br) have been detected in ^{207}Pb NMR spectra of $APbX_3$ perovskites. The coupling strengths are in the range of 400 Hz for $^1J_{Pb\text{-}Cl}$ and 2.3 kHz for $^1J_{Pb\text{-}Br}$. Only $CsPbCl_3$ and $CsPbBr_3$ exhibit pronounced coupling patterns at RT. The substantial diminishing of structural dynamics in $MAPbBr_3$ at temperatures below 150 K results in the resolution of the J-coupling. For the iodine compounds, a coupling $^1J_{Pb\text{-}I}$ of *ca.* 3 kHz can only be postulated based on the overall spectral line width, but it could not be experimentally resolved. Future studies might concentrate on resolving Pb-iodide couplings at lower magnetic fields. ^{207}Pb NMR has shown to be an easily accessible tool to detect permanent and dynamic distortions in the inorganic framework of perovskites. This shows its great potential to better characterize these materials, which is not possible by normal X-ray diffraction. Another important avenue is to probe the relationship between Pb-Br J-couplings and the structural disorder induced by the dimensionality, for instance, in colloidal $CsPbBr_3$ NCs.

Methods

$APbX_3$ (A = Cs, MA, FA; X = Cl, Br, I) compounds were synthesized in the corresponding hydrohalic acid. $CsPbX_3$ was additionally prepared from the solid state by melting together CsX and PbX_2 in a 1:1 ratio. $CsPbBr_3$ NCs were prepared by hot injection using long-chain zwitterionic molecules as capping ligands[83]. See SI for further details. The purity of all compounds was confirmed by powder X-ray diffraction (pXRD). All samples were ground into a fine powder and densely packed into ZrO_2 rotors. Solid-state Magic Angle Spinning (MAS) NMR experiments at ambient conditions were performed on three Bruker Avance IIIHD spectrometers (Bruker Biospin, Fällanden, Switzerland). The 11.7 and 16.4 T instruments were equipped with 2.5 mm two-channel

and three-channel solid-state probe heads. The spinning frequency was set between 0 and 20 kHz. The 14.1 T magnet was equipped with a 3.2 mm double-channel MAS probe and a MAS spinning rate of 10 kHz was used. Low-temperature experiments were conducted on the 14.1 T Bruker instrument equipped with a 3.2 mm double-channel low-temperature MAS probe using MAS spinning of 10 kHz. ^{207}Pb NMR chemical shifts were referenced to $PbMe_4$. A Hahn echo pulse-sequence was used for all measurements with an echo delay between 0.1 and 0.5 ms[96]. The rf field of the echo pulses was set to 35.7, 26.3 and 19.8 kHz at 11.7, 14.1 and 16.4 T, respectively, which is strong enough to be refocused the complete spectra of the 3D phases. The 1D phases are too broad (>140 kHz) to be refocused completely.

Received: 20 February 2020; Accepted: 20 April 2020;
Published online: 19 May 2020

References

1. Yang, W. S. *et al*. High-Performance Photovoltaic Perovskite Layers Fabricated through Intramolecular Exchange. *Science* **348**, 1234–1237 (2015).
2. Yang, W. S. *et al*. Iodide Management in Formamidinium-Lead-Halide–Based Perovskite Layers for Efficient Solar Cells. *Science* **356**, 1376–1379 (2017).
3. Kim, Y. C. *et al*. Printable Organometallic Perovskite Enables Large-Area, Low-Dose X-Ray Imaging. *Nature* **550**, 87 (2017).
4. Yakunin, S. *et al*. Detection of Gamma Photons using Solution-Grown Single Crystals of Hybrid Lead Halide Perovskites. *Nat. Photonics* **10**, 585 (2016).
5. Wei, H. *et al*. Dopant Compensation in Alloyed $CH_3NH_3PbBr_{3-x}Cl_x$ Perovskite Single Crystals for Gamma-Ray Spectroscopy. *Nat. Mater.* **16**, 826 (2017).
6. He, Y. *et al*. High Spectral Resolution of Gamma-Rays at Room Temperature by Perovskite $CsPbBr_3$ Single Crystals. *Nat. Commun.* **9**, 1609 (2018).
7. Sutherland, B. R. & Sargent, E. H. Perovskite Photonic Sources. *Nat. Photonics* **10**, 295 (2016).
8. Kovalenko, M. V., Protesescu, L. & Bodnarchuk, M. I. Properties and Potential Optoelectronic Applications of Lead Halide Perovskite Nanocrystals. *Science* **358**, 745–750 (2017).
9. Xing, J. *et al*. Color-Stable Highly Luminescent Sky-Blue Perovskite Light-Emitting Diodes. *Nat. Commun.* **9**, 3541 (2018).
10. Cao, Y. *et al*. Perovskite Light-Emitting Diodes Based on Spontaneously Formed Submicrometre-Scale Structures. *Nature* **562**, 249–253 (2018).
11. Lin, K. *et al*. Perovskite Light-Emitting Diodes with External Quantum Efficiency Exceeding 20 Per Cent. *Nature* **562**, 245–248 (2018).
12. Zhao, X., Ng, J. D. A. & Friend, R. H. Tan Z.-K. Opportunities and Challenges in Perovskite Light-Emitting Devices. *ACS Photonics* **5**, 3866–3875 (2018).
13. Chiba, T. *et al*. Anion-Exchange Red Perovskite Quantum Dots with Ammonium Iodine Salts for Highly Efficient Light-Emitting Devices. *Nat. Photonics* **12**, 681–687 (2018).
14. Shynkarenko, Y. *et al*. Direct Synthesis of Quaternary Alkylammonium-Capped Perovskite Nanocrystals for Efficient Blue and Green Light-Emitting Diodes. *ACS Energy Lett.* **4**, 2703–2711 (2019).
15. Zakutayev, A. *et al*. Defect Tolerant Semiconductors for Solar Energy Conversion. *J. Phys. Chem. Lett.* **5**, 1117–1125 (2014).
16. Brandt, R. E., Stevanović, V., Ginley, D. S. & Buonassisi, T. Identifying Defect-Tolerant Semiconductors with High Minority-Carrier Lifetimes: Beyond Hybrid Lead Halide Perovskites. *MRS Commun.* **5**, 265–275 (2015).
17. Walsh, A., Scanlon, D. O., Chen, S., Gong, X. G. & Wei, S.-H. Self-Regulation Mechanism for Charged Point Defects in Hybrid Halide Perovskites. *Angew. Chem., Int. Ed.* **54**, 1791–1794 (2015).
18. Comin, R. *et al*. Lattice Dynamics and the Nature of Structural Transitions in Organolead Halide Perovskites. *Phys. Rev. B* **94**, 094301 (2016).
19. Kang, J. & Wang, L.-W. High Defect Tolerance in Lead Halide Perovskite CsPbBr3. *J. Phys. Chem. Lett.* **8**, 489–493 (2017).
20. Tan, H. *et al*. Dipolar Cations Confer Defect Tolerance in Wide-Bandgap Metal Halide Perovskites. *Nat. Commun.* **9**, 3100 (2018).
21. Huang, H., Bodnarchuk, M. I., Kershaw, S. V., Kovalenko, M. V. & Rogach, A. L. Lead Halide Perovskite Nanocrystals in the Research Spotlight: Stability and Defect Tolerance. *ACS Energy Lett.* **2**, 2071–2083 (2017).
22. Kubicki, D. J. *et al*. Cation Dynamics in Mixed-Cation $(MA)_x(FA)_{1-x}PbI_3$ Hybrid Perovskites from Solid-State NMR. *J. Am. Chem. Soc.* **139**, 10055–10061 (2017).
23. Roiland, C. *et al*. Multinuclear NMR as a Tool for Studying Local Order and Dynamics in $CH_3NH_3PbX_3$ (X = Cl, Br, I) Hybrid Perovskites. *Phys. Chem. Chem. Phys.* **18**, 27133–27142 (2016).
24. Senocrate, A. *et al*. The Nature of Ion Conduction in Methylammonium Lead Iodide: A Multimethod Approach. *Angew. Chem., Int. Ed.* **56**, 7755–7759 (2017).
25. Senocrate, A., Moudrakovski, I. & Maier, J. Short-Range Ion Dynamics in Methylammonium Lead Iodide by Multinuclear Solid State NMR and 127I NQR. *Phys. Chem. Chem. Phys.* **20**, 20043–20055 (2018).
26. Wasylishen, R. E., Knop, O. & Macdonald, J. B. Cation Rotation in Methylammonium Lead Halides. *Solid State Commun.* **56**, 581–582 (1985).
27. Bernard, G. M. *et al*. Methylammonium Cation Dynamics in Methylammonium Lead Halide Perovskites: A Solid-State NMR Perspective. *J. Phys. Chem. A* **122**, 1560–1573 (2018).
28. Knop, O., Wasylishen, R. E., White, M. A., Cameron, T. S. & Oort, M. J. M. V. Alkylammonium Lead Halides. Part 2. CH3NH3PbX3 (X = Cl, Br, I) Perovskites: Cuboctahedral Halide Cages with Isotropic Cation Reorientation. *Can. J. Chem.* **68**, 412–422 (1990).
29. Kubicki, D. J. *et al*. Phase Segregation in Cs-, Rb- and K-Doped Mixed-Cation $(MA)_x(FA)_{1-x}PbI_3$ Hybrid Perovskites from Solid-State NMR. *J. Am. Chem. Soc.* **139**, 14173–14180 (2017).
30. Milić, J. V. *et al*. Supramolecular Engineering for Formamidinium-Based Layered 2D Perovskite Solar Cells: Structural Complexity and Dynamics Revealed by Solid-State NMR Spectroscopy. *Adv. Energy Mater.* **9**, 1900284 (2019).
31. Karmakar, A. *et al*. Mechanochemical Synthesis of 0D and 3D Cesium Lead Mixed Halide Perovskites. *Chem. Commun.* **55**, 5079–5082 (2019).
32. Ray, A. *et al*. Green-Emitting Powders of Zero-Dimensional Cs4PbBr6: Delineating the Intricacies of the Synthesis and the Origin of Photoluminescence. *Chem. Mater.* **31**, 7761–7769 (2019).
33. Rosales, B. A. *et al*. Persistent Dopants and Phase Segregation in Organolead Mixed-Halide Perovskites. *Chem. Mater.* **28**, 6848–6859 (2016).
34. Franssen, W. M. J. & Kentgens, A. P. M. Solid–state NMR of hybrid halide perovskites. *Solid State Nucl. Magn. Reson.* **100**, 36–44 (2019).
35. Zhu, H. *et al*. Screening in Crystalline Liquids Protects Energetic Carriers in Hybrid Perovskites. *Science* **353**, 1409–1413 (2016).
36. Eames, C. *et al*. Ionic Transport in Hybrid Lead Iodide Perovskite Solar Cells. *Nat. Commun.* **6**, 7497 (2015).

37. Mosconi, E. & De Angelis, F. Mobile Ions in Organohalide Perovskites: Interplay of Electronic Structure and Dynamics. *ACS Energy Lett.* **1**, 182–188 (2016).
38. Gallop, N. P. *et al*. Rotational Cation Dynamics in Metal Halide Perovskites: Effect on Phonons and Material Properties. *J. Phys. Chem. Lett.* **9**, 5987–5997 (2018).
39. Whalley, L. D., Skelton, J. M., Frost, J. M. & Walsh, A. Phonon Anharmonicity, Lifetimes, and Thermal Transport in $CH_3NH_3PbI_3$ from Many-Body Perturbation Theory. *Phys. Rev. B* **94**, 220301 (2016).
40. Beecher, A. N. *et al*. Direct Observation of Dynamic Symmetry Breaking above Room Temperature in Methylammonium Lead Iodide Perovskite. *ACS Energy Lett.* **1**, 880–887 (2016).
41. Marronnier, A. *et al*. Structural Instabilities Related to Highly Anharmonic Phonons in Halide Perovskites. *J. Phys. Chem. Lett.* **8**, 2659–2665 (2017).
42. Marronnier, A. *et al*. Anharmonicity and Disorder in the Black Phases of Cesium Lead Iodide Used for Stable Inorganic Perovskite Solar Cells. *ACS Nano* **12**, 3477–3486 (2018).
43. Baikie, T. *et al*. A Combined Single Crystal Neutron/X-ray Diffraction and Solid-State Nuclear Magnetic Resonance Study of the Hybrid Perovskites $CH_3NH_3PbX_3$ (X = I, Br and Cl). *J. Mater. Chem. A* **3**, 9298–9307 (2015).
44. Franssen, W. M. J., van Es, S. G. D., Dervişoğlu, R., de Wijs, G. A. & Kentgens, A. P. M. Symmetry, Dynamics, and Defects in Methylammonium Lead Halide Perovskites. *J. Phys. Chem. Lett.* **8**, 61–66 (2017).
45. Franssen, W. M. J., Bruijnaers, B. J., Portengen, V. H. L. & Kentgens, A. P. M. Dimethylammonium Incorporation in Lead Acetate Based $MAPbI_3$ Perovskite Solar Cells. *Chem. Phys. Chem.* **19**, 3107–3115 (2018).
46. Armstrong, R. L., Lourens, J. A. J. & Stroud, J. D. 133Cs Spin-Lattice Relaxation Study of Phase Transitions in $CsPbCl_3$. *Phys. Rev. B* **13**, 5099–5101 (1976).
47. Chen, Y. *et al*. Surface Termination of $CsPbBr_3$ Perovskite Quantum Dots Determined by Solid-State NMR Spectroscopy. *J. Am. Chem. Soc.* **142**, 6117–6127 (2020).
48. Boziki, A. *et al*. Atomistic Origins of the Limited Phase Stability of Cs^+-Rich $FA_xCs_{(1-x)}PbI_3$ Mixtures. *Chem. Mater.* **32**, 2605–2614 (2020).
49. Kubicki, D. J. *et al*. Doping and phase segregation in Mn^{2+}- and Co^{2+}-doped lead halide perovskites from 133Cs and 1H NMR relaxation enhancement. *J. Mater. Chem. A* **7**, 2326–2333 (2019).
50. Prochowicz, D. *et al*. One-Step Mechanochemical Incorporation of an Insoluble Cesium Additive for High Performance Planar Heterojunction Solar Cells. *Nano Energy* **49**, 523–528 (2018).
51. Kubicki, D. J. *et al*. Phase Segregation in Potassium-Doped Lead Halide Perovskites from 39K Solid-State NMR at 21.1 T. *J. Am. Chem. Soc.* **140**, 7232–7238 (2018).
52. Schurko, R. W. *Acquisition of Wideline Solid-State NMR Spectra of Quadrupolar Nuclei* (ed. Grant, D. M., Harris, R. K.) 77–90 (John Wiley & Sons Ltd, 2011).
53. Wasylishen, R. E., Ashbrook S. E., & Wimperis, S. *NMR of Quadrupolar Nuclei in Solid Materials* (John Wiley & Sons Ltd, 2012).
54. Tovborg-Jensen, N. NQR Investigation of Phase Transitions in Cesium Plumbochloride. *J. Chem. Phys.* **50**, 559–560 (1969).
55. Volkov, A. F., Venevtsev, Y. N. & Semin, G. K. Nuclear Quadrupole Resonance (NQR) of 79Br and 81Br in Perovskite and Orthorhombic Forms of $CsPbBr_3$ and $CsPbJ_3$. *Phys. Status Solidi B* **35**, K167–K169 (1969).
56. Armstrong, R. L. Pure Nuclear Quadrupole Resonance Studies of Structural Phase Transitions. *J. Magn. Reson. (1969-1992)* **20**, 214–231 (1975).
57. Hidaka, M., Okamoto, Y. & Zikumaru, Y. Structural Phase Transition of $CsPbCl_3$ below Room Temperature. *Phys. Status Solidi A* **79**, 263–269 (1983).
58. Sharma, S., Weiden, N., Weiss, A. Phase Transitions in $CsSnCl_3$ and $CsPbBr_3$ An NMR and NQR Study. In: Z. Naturforsch. A) (1991).
59. Sharma, S., Weiden, N., Weiss, A. 207Pb and 205Tl NMR on Perovskite Type Crystals $APbX_3$ (A = Cs, Tl, X = Br, I). In: Z. Naturforsch. A) (1987).
60. Ullmann, H. Strukturchemische und MAS-NMR-Spektroskopische Untersuchungen mit Quantenchemischen Berechnungen von Binären, *Ternären und Quaternären Blei(II)-Halogeniden* (Herbert Utz Verlag Wissenschaft, 1998).
61. Askar, A. M., Bernard, G. M., Wiltshire, B., Shankar, K. & Michaelis, V. K. Multinuclear Magnetic Resonance Tracking of Hydro, Thermal, and Hydrothermal Decomposition of $CH_3NH_3PbI_3$. *J. Phys. Chem. C* **121**, 1013–1024 (2017).
62. Rosales, B. A. *et al*. Lead Halide Perovskites: Challenges and Opportunities in Advanced Synthesis and Spectroscopy. *ACS Energy Lett.* **2**, 906–914 (2017).
63. Bernard, G. M. *et al*. Methylammonium Lead Chloride: A Sensitive Sample for an Accurate NMR Thermometer. *J. Magn. Reson.* **283**, 14–21 (2017).
64. Nazarenko, O. *et al*. Guanidinium-Formamidinium Lead Iodide: A Layered Perovskite-Related Compound with Red Luminescence at Room Temperature. *J. Am. Chem. Soc.* **140**, 3850–3853 (2018).
65. Hanrahan, M. P., Men, L., Rosales, B. A., Vela, J. & Rossini, A. J. Sensitivity-Enhanced 207Pb Solid-State NMR Spectroscopy for the Rapid, Non-Destructive Characterization of Organolead Halide Perovskites. *Chem. Mater.* **30**, 7005–7015 (2018).
66. Hahn, E. L. & Maxwell, D. E. Spin Echo Measurements of Nuclear Spin Coupling in Molecules. *Phys. Rev.* **88**, 1070–1084 (1952).
67. Goesten, M. G. & Hoffmann, R. Mirrors of Bonding in Metal Halide Perovskites. *J. Am. Chem. Soc.* **140**, 12996–13010 (2018).
68. Taylor, R. E., Beckmann, P. A., Bai, S. & Dybowski, C. 127I and 207Pb Solid-State NMR Spectroscopy and Nuclear Spin Relaxation in PbI2: A Preliminary Study. *J. Phys. Chem. C* **118**, 9143–9153 (2014).
69. Kennedy, J. D., McFarlane, W. & Wrackmeyer, B. Indirect Nuclear Spin-Spin Coupling of Lead-207 to Other Magnetic Nuclei. *Inorg. Chem.* **15**, 1299–1302 (1976).
70. Glatfelter, A. *et al*. Solid-State 207Pb NMR Studies of Mixed Lead Halides, PbFX (X=Cl, Br, or I). *Spectrochim. Acta, Part A* **66**, 1361–1363 (2007).
71. Sendner, M. *et al*. Optical Phonons in Methylammonium Lead Halide Perovskites and Implications for Charge Transport. *Mater. Horiz.* **3**, 613–620 (2016).
72. Yang, R. X., Skelton, J. M., da Silva, E. L., Frost, J. M. & Walsh, A. Spontaneous Octahedral Tilting in the Cubic Inorganic Cesium Halide Perovskites CsSnX3 and CsPbX3 (X = F, Cl, Br, I). *J. Phys. Chem. Lett.* **8**, 4720–4726 (2017).
73. Bechtel, J. S. & Van der Ven, A. Octahedral Tilting Instabilities in Inorganic Halide Perovskites. *Phys. Rev. Mater.* **2**, 025401 (2018).
74. Autschbach, J. & Le Guennic, B. Analyzing and Interpreting NMR Spin–Spin Coupling Constants Using Molecular Orbital Calculations. *J. Chem. Educ.* **84**, 156 (2007).
75. Martineau, C., *et al*. Accurate Heteronuclear J-Coupling Measurements in Dilute Spin Systems using the Multiple-Quantum Filtered J-Resolved Experiment. *Chem. Commun*., 2720–2722 (2007).
76. Yu, H. *et al*. Solid-State ^{63}Cu, ^{65}Cu, and ^{31}P NMR Spectroscopy of Photoluminescent Copper(I) Triazole Phosphine Complexes. *J. Phys. Chem. A* **119**, 8279–8293 (2015).
77. Massiot, D. *et al*. Detection and Use of small J Couplings in Solid State NMR Experiments. *Comptes Rendus Chimie* **13**, 117–129 (2010).
78. Kamieńska-Trela, K., Wójcik, J. Applications of spin-spin couplings. In: *Nuclear Magnetic Resonance*: Volume 41. The Royal Society of Chemistry (2012).
79. Wells, H. L. Über die Cäsium- und Kalium-Bleihalogenide. *Z. Anorg. Allg. Chem.* **3**, 195–210 (1893).

80. Nazarenko, O., Yakunin, S., Morad, V., Cherniukh, I. & Kovalenko, M. V. Single Crystals of Caesium Formamidinium Lead Halide Perovskites: Solution Growth and Gamma Dosimetry. *NPG Asia Mater.* **9**, e373 (2017).
81. Møller, C. K. Crystal Structure and Photoconductivity of Cæsium Plumbohalides. *Nature* **182**, 1436 (1958).
82. Trots, D. M. & Myagkota, S. V. High-Temperature Structural Evolution of Caesium and Rubidium Triiodoplumbates. *J. Phys. Chem. Solids* **69**, 2520–2526 (2008).
83. Krieg, F. *et al*. Colloidal $CsPbX_3$ (X = Cl, Br, I) Nanocrystals 2.0: Zwitterionic Capping Ligands for Improved Durability and Stability. *ACS Energy Lett.* **3**, 641–646 (2018).
84. Becker, E. D. *High Resolution NMR* (Second Edition) (Academic Press, 1980).
85. Lowe, I. J. Free Induction Decays of Rotating Solids. *Phys. Rev. Lett.* **2**, 285–287 (1959).
86. Rodová, M., Brožek, J., Knížek, K. & Nitsch, K. Phase Transitions in Ternary Cesium Lead Bromide. *J. Therm. Anal. Calorim.* **71**, 667–673 (2003).
87. Stoumpos, C. C. *et al*. Crystal Growth of the Perovskite Semiconductor $CsPbBr_3$: A New Material for High-Energy Radiation Detection. *Cryst. Growth Des.* **13**, 2722–2727 (2013).
88. Wang, K.-H., Li, L.-C., Shellaiah, M. & Wen Sun, K. Structural and Photophysical Properties of Methylammonium Lead Tribromide ($MAPbBr_3$) Single Crystals. *Sci. Rep.* **7**, 13643 (2017).
89. Even, J., Carignano, M. & Katan, C. Molecular Disorder and Translation/Rotation Coupling in the Plastic Crystal Phase of Hybrid Perovskites. *Nanoscale* **8**, 6222–6236 (2016).
90. Bernasconi, A. & Malavasi, L. Direct Evidence of Permanent Octahedra Distortion in $MAPbBr_3$ Hybrid Perovskite. *ACS Energy Lett.* **2**, 863–868 (2017).
91. Schueller, E. C. *et al*. Crystal Structure Evolution and Notable Thermal Expansion in Hybrid Perovskites Formamidinium Tin Iodide and Formamidinium Lead Bromide. *Inorg. Chem.* **57**, 695–701 (2018).
92. Protesescu, L. *et al*. Monodisperse Formamidinium Lead Bromide Nanocrystals with Bright and Stable Green Photoluminescence. *J. Am. Chem. Soc.* **138**, 14202–14205 (2016).
93. Futscher, M. H. *et al*. Quantification of Ion Migration in $CH_3NH_3PbI_3$ Perovskite Solar Cells by Transient Capacitance Measurements. *Mater. Horiz.* **6**, 1497–1503 (2019).
94. Møller C. K. *On the structure of caesium hexahalogeno-plumbates (II)* (Munksgaard, 1960).
95. Bertolotti, F. *et al*. Coherent Nanotwins and Dynamic Disorder in Cesium Lead Halide Perovskite Nanocrystals. *ACS Nano* **11**, 3819–3831 (2017).
96. Hahn, E. L. Spin Echoes. *Phys. Rev.* **80**, 580–594 (1950).

Author contributions

M.K. and R.V. supervised this work. M.A. and L.P. carried out NMR experiments and analyzed the results. O. N., B.B., and F.K. synthesized all samples. M. A. and M. K. wrote the manuscript with the input of all co-authors.

Competing interests

The authors declare no competing interests.

Additional information

Supplementary information is available for this paper at https://doi.org/10.1038/s41598-020-65071-4.

Correspondence and requests for materials should be addressed to R.V. or M.V.K.

Reprints and permissions information is available at www.nature.com/reprints.

Publisher's note Springer Nature remains neutral with regard to jurisdictional claims in published maps and institutional affiliations.